*Journal of The Electrochemical Society*, **160** (9) A1611-A1617 (2013)
0013-4651/2013/160(9)/A1611/7/$31.00 © The Electrochemical Society


# Nanocomposites of Titanium Dioxide and Polystyrene-Poly(ethylene oxide) Block Copolymer as Solid-State Electrolytes for Lithium Metal Batteries

**Inna Gurevitch,[a] Raffaella Buonsanti,[b] Alexander A. Teran,[a,c,*] Bernd Gludovatz,[d] Robert O. Ritchie,[d] Jordi Cabana,[a,**,z] and Nitash P. Balsara[a,d,e,z]**

[a]*Environmental Energy Technologies Division, Lawrence Berkeley National Laboratory, Berkeley, California 94720, USA*
[b]*The Molecular Foundry, Lawrence Berkeley National Laboratory, Berkeley, California 94720, USA*
[c]*Department of Chemical & Biomolecular Engineering, University of California, Berkeley, Berkeley, California 94720, USA*
[d]*Materials Sciences Division, Lawrence Berkeley National Laboratory, Berkeley, California 94720, USA*
[e]*Department of Chemistry, University of Illinois at Chicago, Chicago, Illinois 60607, USA*

There is considerable interest in developing solid electrolytes for rechargeable lithium batteries as they have the potential to increase both energy density due to incorporation of a lithium metal anode and safety of batteries due to the fact that they are nonflammable. Block copolymers with a mechanically hard non-conducting block and a soft ion-conducting block provide an avenue for obtaining highly conducting rigid solids. In this study we add surface-modified $TiO_2$ nanoparticles to a mixture of polystyrene-*block*-poly(ethylene oxide) and bis(trifluoromethane)sulfonimide lithium salt. The presence of $BF_4^-$ moieties on the surface of the particles was essential for obtaining macroscopically homogeneous electrolytes; macrophase separation was observed with the same nanoparticles with surfaces covered with oleic acid. The stability of these composite electrolytes against lithium metal electrodes was tested in symmetric lithium-composite electrolyte-lithium cells. The surprising result was that electrolytes with 24 wt% nanoparticles exhibited optimum stability; the amount of charge passed before dendrite formation observed in the optimized composite electrolyte was a factor of 4.7 larger than that of the neat block copolymer electrolyte. Both tensile and shear moduli of the electrolytes were non-monotonic functions of particle concentration with peaks in the vicinity of 17 to 20 wt%.
 [DOI: 10.1149/2.117309jes] 

Manuscript submitted May 22, 2013; revised manuscript received July 8, 2013. Published July 23, 2013. This was Paper 1202 presented at the Honolulu, Hawaii, Meeting of the Society, October 7–12, 2012.

There is considerable interest in developing solid polymer electrolytes for rechargeable lithium batteries. The electrolyte used in today's lithium batteries is a mixture of flammable alkyl carbonate solvents and lithium salts. Replacing the liquid solvents with a solid polymer has the potential to improve both safety and energy density of the batteries.[1,2] Much of the work on solid electrolytes is based on mixtures of poly(ethylene oxide) (PEO) and lithium salts.[2–6] Safety is enhanced due to the non-flammable nature of PEO. The capacity of lithium anodes is significantly higher than that of graphite-based anodes used in current batteries.[1] Theoretical predictions indicate that solid electrolytes with sufficiently high ionic conductivity and elastic moduli are necessary to prevent the growth of dendrites on the surface of the lithium anode.[7] Dendritic growth can short circuit batteries and result in explosive battery failure. A standard approach for increasing the moduli of polymers is by adding solid particles.[6,8–14]

While there is no doubt that the dispersion of solid particles increases the modulus of polymers, its effect on ionic conductivity is controversial. Some early reports suggested that the addition of ceramic particles increases the ionic conductivity of PEO/salt mixtures by one to four orders of magnitudes.[8,11] It was, however, unclear if the electrolytes studied in refs. 8 and 11 were prepared under water-free conditions. The hygroscopic nature of the lithium salt may result in significant water contamination which, in turn, affects ion transport. Surface hydroxyl groups found on ceramics such as $TiO_2$ are also capable of absorbing water from the surrounding air. The conductivities of composite polymer/ceramic electrolytes prepared under water-free conditions were only marginally higher than those of PEO/salt mixtures.[9,10,12] Takahashi et al. have shown that the ionic conductivity of lithium aluminum titanium phosphate (LATP) pellets decreases after drying under argon atmosphere.[15] The conductivity of hybrid electrolytes based on an ionic liquid covalently tethered to silica nanoparticles also decreases with increasing nanoparticle content.[16,17] The effect of ceramic particle addition on the conductivity of polymer electrolytes is thus an open question.

In this work, we study the effect of adding ceramic nanoparticles to block copolymer/salt mixtures, and evaluate their properties as solid electrolytes. Symmetric polystyrene-*block*-poly(ethylene oxide) (SEO) copolymers were synthesized using living anionic polymerization.[18–20] Polymer electrolytes were prepared by mixing SEO and bis(trifluoromethane)sulfonimide lithium salt (LiTFSI). The block copolymers self-assemble into continuous nanodomains, wherein the soft poly(ethylene oxide) (PEO) nanodomains conduct ions, while the hard polystyrene (PS) nanodomains increase the modulus of the electrolyte. Ionic conductivity of $10^{-4}$ S/cm combined with shear modulus of about $10^8$ Pa were reported for high molecular weight SEO block copolymers at 90°C.[19–21] SEO/LiTFSI solid electrolytes with lamellar block copolymer morphology enable resolution of the conflicting requirements of high modulus, needed for decreasing dendrite growth from the lithium electrode,[7,22] and interfacial adhesion, needed for maintaining contact between the lithium anode and the electrolyte.[21] The stability of the electrode-electrolyte interface was enhanced in SEO-based block copolymer electrolytes relative to PEO-based homopolymer electrolytes.[21]

The objective of this paper is to explore the properties of mixtures of ceramic particles/SEO/LiTFSI. We first report on the effect of the ceramic particles on the electrolyte's morphology. We then show that the addition of ceramic particles decreases the ionic conductivity of the composite electrolyte. In spite of this, the stability of the electrode-electrolyte interface is enhanced by the presence of ceramic particles. This is attributed to an increase in modulus and changes in electrolyte morphology.

## Experimental

*$TiO_2$ nanoparticle synthesis.*— The $TiO_2$ synthesis was carried out under air-free conditions using a standard Schlenk line setup. 35 g of oleic acid (Sigma-Aldrich) were heated to 110°C under vacuum for 40 min, followed by cooling to 60°C. 2.5 mL of titanium isopropoxide (Ti precursor, Sigma-Aldrich) and a solution of 0.5 g of trimethylamine N-oxide dehydrate (Sigma-Aldrich) dissolved in 2.5 mL water were added to the oleic acid. The temperature of the reaction mixture was increased to 95°C under nitrogen. The reaction was allowed to proceed for 4 days at this temperature. The $TiO_2$ nanopar-

*Electrochemical Society Student Member.
**Electrochemical Society Active Member.
zE-mail: jcabana@uic.edu; nbalsara1@gmail.com

ticles (NPs) thus obtained were covered with oleic acid. These NPs were precipitated in ethanol and concentrated by centrifugation. The NPs which were isolated at the bottom of the centrifuge tubes were dispersed in hexane. The precipitation and re-dispersion process was repeated to eliminate the excess oleic acid. The NP dispersion in hexane is stable. Since oleic acid is hydrophobic, dispersing the as-synthesized NPs in SEO would result in preferential segregation of the NPs in the PS domains. We thus performed a ligand exchange reaction on the NPs. *N,N*-Dimethylformamide (DMF) was added to the $TiO_2$ NPs dispersed in hexane, resulting in a phase-separated mixture. A few crystals of nitrosyl tetrafluoroborate ($NOBF_4$, Sigma-Aldrich) were added to the phase-separated mixture. After 2 min of stirring, the mixture was precipitated in toluene, centrifuged, and dispersed in DMF. The precipitation and re-dispersion process was repeated three times to wash off oleic acid. The final product of the synthesis was a stable dispersion of $TiO_2$ NPs with $BF_4^-$ groups on the surface in DMF.[23,24] Positively charged metal centers on or near the surface ensure that the NPs are electrically neutral.[23] Completion of the ligand exchange reaction was confirmed by infra-red spectroscopy, which showed the disappearance of peaks associated with oleic acid and the appearance of peaks associated with $BF_4^-$ groups. The infra-red signatures obtained were similar to those reported in the literature.[23]

*$TiO_2$-SEO block copolymer nanocomposite preparation.*— All sample preparation and experiments, except for measurement of mechanical properties, were performed in an argon filled glove box with less than 1 ppm water content and less than 3 ppm oxygen content. SEO block copolymers were synthesized on a vacuum line using sequential anionic polymerization.[19] The SEO block copolymer used for the nanocomposite preparation had a poly(ethylene oxide) block molecular weight of 63 kg/mol and a polystyrene block molecular weight of 60 kg/mol. The LiTFSI salt was added to a mixture of SEO and 1-methyl-2-pyrrolidone (NMP); the solid content of the solution was 1.3 wt%. The molar ratio of Li to ethylene oxide moieties was 0.085. SEO/$TiO_2$ membranes for the measurement of mechanical properties were prepared without LiTFSI salt due to the hygroscopic nature of the salt and the lack of availability of instruments to measure mechanical properties in a water-free environment. In reference 19 it was shown that the addition of small amounts of the LiTFSI salt has no detrimental effect on the mechanical properties of the SEO-based electrolytes.

Different amounts of the $TiO_2$ NPs in DMF were added to the NMP/SEO/LiTFSI mixtures. The resulting solutions were heated (~60°C) and stirred overnight. Membranes with thicknesses ranging from 10 to 30 μm were obtained by casting and drying the solutions. The electrolytes were dried overnight under vacuum at 90°C. The NP content in the dried SEO/LiTFSI/$TiO_2$ electrolyte was determined using thermal gravimetric analysis (TGA Q5000) wherein the samples were heated to 600°C in air using a heating rate of 10°C/min. SEO/LiTFSI mixtures were subjected to the same thermal gravimetric analysis to determine the mass of residues resulting from the decomposition of LiTFSI (about 2.5 wt%). The mass of residues was subtracted from the TGA results of $TiO_2$/SEO/LiTFSI mixtures to give the mass fraction of $TiO_2$ in the composite electrolytes. Samples for electrochemical measurements are labeled SEO/Li/T-xx and are listed in Table I. Samples for mechanical measurements are labeled SEO/T-xx and are listed in Table II. In both labels, xx is the weight percent of NPs in the electrolytes. Identical casting procedures were used to prepare the samples listed in Table I and Table II. In spite of this, NP content of the SEO/Li/T series is slightly different from that of SEO/T series (see Table I and Table II). This is probably due to the fact that different batches of the NP/DMF dispersions were used to prepare the samples.

**Table I. Properties of SEO/LiTFSI/$TiO_2$ electrolytes used in cycling studies.**

| Sample | Average Thickness (μm) | Appearance | Average $C_d$ (C/cm$^2$) |
|---|---|---|---|
| SEO/Li/T-0 | 23 ± 2 | Transparent | 374 ± 86 |
| SEO/Li/T-3.9 | 14 ± 2 | Transparent | 236 ± 115 |
| SEO/Li/T-11.5 | 11 ± 2 | Opaque | 1064 ± 547 |
| SEO/Li/T-23.9 | 24 ± 5 | Transparent | 1766 ± 445 |
| SEO/Li/T-27.9 | 19 ± 2 | Opaque | 259 ± 240 |

**Table II. Mechanical properties of SEO and SEO/$TiO_2$ composites.**

| Sample | Tensile Modulus, $E$ (Pa), at 25°C | Storage Shear Modulus, $G'$, (Pa), at 90°C |
|---|---|---|
| SEO/T-0 | $3.6 \cdot 10^8$ | $2.4 \cdot 10^7$ |
| SEO/T-4.6 | $7.7 \cdot 10^8$ | $4.2 \cdot 10^7$ |
| SEO/T-10.6 | $9.1 \cdot 10^8$ | $4.6 \cdot 10^7$ |
| SEO/T-17.4 | $1.3 \cdot 10^9$ | — |
| SEO/T-20.2 | $7.3 \cdot 10^8$ | $7.6 \cdot 10^7$ |
| SEO/T-23.9 | — | $4.3 \cdot 10^7$ |
| SEO/T-25.2 | $6.3 \cdot 10^8$ | $2.7 \cdot 10^7$ |

*Electron microscopy.*— Transmission electron micrographs of $TiO_2$ NP dispersion in hexane were obtained on a Zeiss LIBRA operating at 200 kV. The samples were drop-cast on ultrathin carbon film coated copper grids.

Scanning electron micrographs were obtained on Zeiss ULTRA 55 analytical SEM operating at 5 kV. SEO/LiTFSI/$TiO_2$ samples were made by drop casting solutions described above on nickel foils to decrease charging effects under the electron beam.

*X-ray scattering.*— Resonance soft X-ray scattering (RSoXS) experiments were performed at beamline 11.0.2 at the Advanced Light Source (ALS) at Lawrence Berkeley National Laboratory (LBNL) to determine the structure of the electrolyte membranes. A 1.3 wt% solution of SEO/LiTFSI and SEO/LiTFSI/$TiO_2$ mixtures in NMP were drop casted on 200 nm thickness silicon nitride windows. 2D profiles were recorded on a Princeton Instrument PI-MTE in-vacuum camera using an incident X-ray beam with energy of 282 eV (in the vicinity of the carbon edge).[25,26] The scattering intensity is presented as a function of the magnitude of the scattering vector, $q$, where $q = 4\pi \sin(\theta/2)/\lambda$, where $\theta$ is the scattering angle and $\lambda$ is the wavelength of the X-rays. We used RSoXS instead of small-angle X-ray scattering to access the low-$q$ regime.

*Mechanical properties.*— Uniaxial tensile tests were performed under ambient conditions (25°C) to determine stress-strain curves and specifically to measure the tensile Young modulus $E$ values using an MTS Tytron 250 testing machine (MTS Corp., Eden Prairie, MN), operating at a displacement rate of 50 μm/sec with a 5 N load cell. For these measurements, SEO and SEO/$TiO_2$ membranes with thicknesses ranging from 10 to 30 μm, and width ranging from 35 to 65 mm were prepared. The membranes were clamped to produce initial lengths ranging from 10 to 30 mm.

Low-strain measurements were performed using frequency-dependent oscillatory shear tests on an ARES rheometer (Rheometric Scientific) to record the storage and loss shear moduli at 90°C using 8 mm diameter parallel plates. For these measurements, SEO and SEO/$TiO_2$ disks with thicknesses ranging from 400 to 700 μm were prepared. The frequency sweep tests were performed at 0.1% strain to ensure linear response.

*Conductivity measurements and galvanostatic cycling.*— For ionic conductivity measurements, electrolyte membranes were prepared within an insulating spacer with an inner diameter of 3.88 mm. Stainless steel blocking electrodes and aluminum foil current collectors were used to assemble the cells. The electrochemical cell was sealed in a pouch to isolate it from air. The electrolyte thickness was

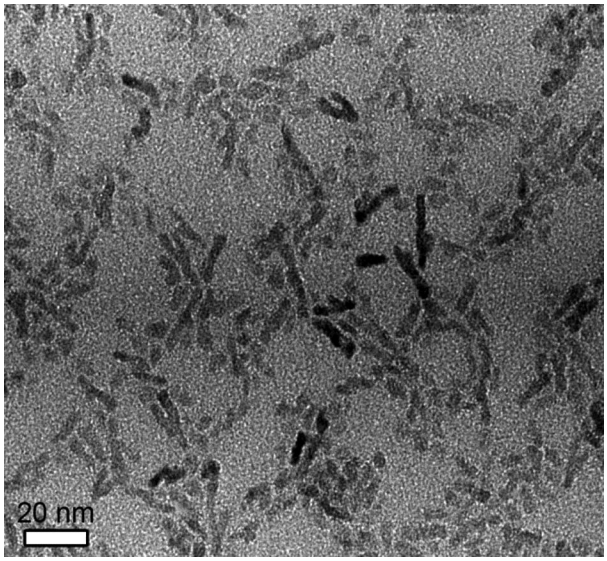


**Figure 1.** TEM micrograph of $TiO_2$ nanorods dispersed in hexane.

measured after conductivity testing and for all cases the thickness was between 250 and 400 μm. Impedance spectroscopy measurements were made using a potentiostat (Bio-Logic VMP3) over frequencies from 1 MHz to 1 Hz, using a peak-to-peak amplitude voltage of 50 mV. Sample conductivities were calculated from the measured sample thickness, the cross-sectional area of the electrolyte, and electrolyte resistances as determined by the low-frequency minima on Nyquist impedance plots.[21]

Symmetric Li-Li cells were used to study dendrite growth, as described in previous work.[21] Lithium foil disks were placed on both sides of the electrolyte membrane, followed by nickel foil current collectors. The electrochemical cell was sealed in a pouch to isolate the cell from the air, and cycled in a heated oven at 90°C.[21] The cell areas were 0.32 and 0.5 $cm^2$. Cycling experiments were performed using a Maccor with a constant current density of 0.17 $mA/cm^2$ with each half cycle lasting for 4 h. Cells were cycled to a sudden and substantial voltage drop (usually greater than 90%) which remained for several cycles. We take this drop as a signature of the formation of a dendrite short. The charge that had passed through the cell up to the initial drop, $C_d$, was recorded and averaged over different cells (a minimum of three independent cells).

## Results and Discussion

Figure 1 shows a TEM micrograph of the $TiO_2$ NPs used in this study. The NPs are rod-like with an average length of 11 nm and an average diameter of 3 nm. Most of the NPs are anisotropic with length significantly larger than the diameter. The length varies from 5 to 21 nm. In contrast, the diameter of most NPs is very close to 3 nm. The NPs used in this study are similar to those reported in reference 27.

The characteristics of the SEO/LiTFSI and SEO/LiTFSI/$TiO_2$ electrolytes used in this study are summarized in Table I. The same casting procedure was used for all samples. The difference in electrolyte thicknesses is a reflection of a lack of understanding of the relationship between film thickness and the rheological properties of the casting solutions. The SEO/LiTFSI/$TiO_2$ membranes were macroscopically homogeneous with yellowish color. It is worth noting that SEO/LiTFSI/$TiO_2$ membranes were significantly easier to handle than SEO/LiTFSI, i.e. the surface-modified $TiO_2$ containing membranes were a lot less fragile than those without $TiO_2$ NPs.

Adding surface-modified $TiO_2$ NPs to SEO/LiTFSI mixtures has a dramatic effect on morphology. In Figure 2a we show an SEM micrograph of sample SEO/Li/T-0, the SEO/LiTFSI mixture without NPs. A lamellar morphology resulting from microphase separation of the PEO and PS blocks can be clearly seen in Figure 2a. This is consistent with previous work on SEO/LiTFSI mixtures.[19] The sample with 4.3 wt% NPs also exhibited lamellar morphology, although the lamellae are more disordered (Figure 2b). $TiO_2$ NPs appeared bright in the SEM images in Figure 2 due to the high atomic number of Ti, as confirmed by energy dispersive X-ray spectroscopy (EDS) on SEM (the data are not shown). Increasing the NP content to 11.5 wt% resulted in the formation of $TiO_2$ clusters (Figure 2c), and the lamellar phase is no longer evident (Figure 2c-2e). Clustering of $TiO_2$ NPs in block copolymers has been reported in previous studies.[28–31] A further increase of NP content to 23.9 wt% led to the formation of a more homogeneous morphology (Figure 2d), whereas small voids formed in the sample with 25.2 wt% NP content (Figure 2e). It is unclear why sample SEO/Li/T-23.9 appeared more homogeneous than SEO/Li/T-11.5 in the SEM. It is interesting to note that SEO/Li/T-23.9 was significantly more transparent (Figure 2d) than SEO/Li/T-11.5 (Figure 2c).

Representative RSoXS data from SEO/Li/T electrolytes are shown in Figure 3. A well-defined primary peak at $q = q^* = 0.083$ $nm^{-1}$ in SEO/Li/T-0 indicates the presence of a microphase-separated structure.[19] The higher order peaks in the vicinity of $3q^*$ and $4q^*$ are consistent with a lamellar morphology. The expected higher order peak at $2q^*$ is missing, and a scattering shoulder is evident in the vicinity $q = 0.15$ $nm^{-1}$. We are not sure of the origin of these observations. Analysis of the RSoXS data from SEO/Li/T-0 resulted in a domain spacing (center-to-center distance between adjacent PEO lamellae) of 76 nm, in agreement with the SEM micrograph in Figure 2a and with previous studies on SEO electrolytes.[18,19] The RSoXS data from SEO/Li/T-4.3 exhibited a well-defined primary peak at $q = q^* = 0.083$ $nm^{-1}$ with no higher order peaks, consistent with the lack of long-range order in the lamellar morphology observed by SEM (Figure 2b). Primary scattering peaks, usually taken as signatures of microphase separation in block copolymers, are absent in SEO/Li/T-8.9 and SEO/Li/T-22.3 (Figure 3), consistent with the SEM micrographs (Figure 2c-2e).

The tensile properties of SEO and SEO/$TiO_2$ mixtures are shown in Figure 4. (We do not add lithium salt to our samples because these experiments were conducted under ambient conditions.) The strain required to fracture the SEO sample was considerably larger than that for SEO/$TiO_2$ mixtures. The addition of $TiO_2$ NPs had a non-monotonic effect on the stress-strain curves. At a given strain, stress increased with increasing NP content until the SEO/T-17.4. A decrease was observed at higher contents (Figure 5). The tensile moduli, $E$, of the samples were calculated using the low strain data. The results are shown in Figure 5 and clearly show that the room temperature tensile modulus is maximized at around 17.4 wt%. However, such NP contents also act to elevate the strength but to markedly diminish the ductility (Figure 4).

Although the tensile tests reflect mechanical behavior over a large range of strains, the measurements were restricted to room temperature due to instrument limitations. However, our cycling experiments were conducted at 90°C. We thus measured the storage and loss shear moduli, $G'$ and $G''$, of the SEO/$TiO_2$ mixtures as a function of frequency, ω, at 90°C. These data are shown in Figure 6. The storage modulus was found to be a non-monotonic function of $TiO_2$ content. Figure 7 depicts $G'$ of different samples at 10 Hz frequency at 90°C. Adding NPs increased $G'$ when the wt% was less than 20.2%. Higher NP weight fractions resulted in lower values of $G'$. It is evident that NP wt% of about 20% is optimal for improvement of the mechanical properties of the composite electrolytes.

Figure 8 shows the ionic conductivity of SEO/Li/T electrolytes at 90°C. It is evident that adding the $TiO_2$ NPs decreased the ionic conductivity of the electrolytes. The conductivity of SEO/Li/T-4.3 is a factor of three lower than that of SEO/Li/T-0. However, increasing the $TiO_2$ content beyond this value had little effect on ionic conductivity until SEO/Li/T-27.9, which showed a factor of about twenty lower ionic conductivity than SEO/Li/T-0. These observations are different from reports in previous studies on the addition of a variety of ceramic particles to homopolymer-PEO electrolytes.[8–12]

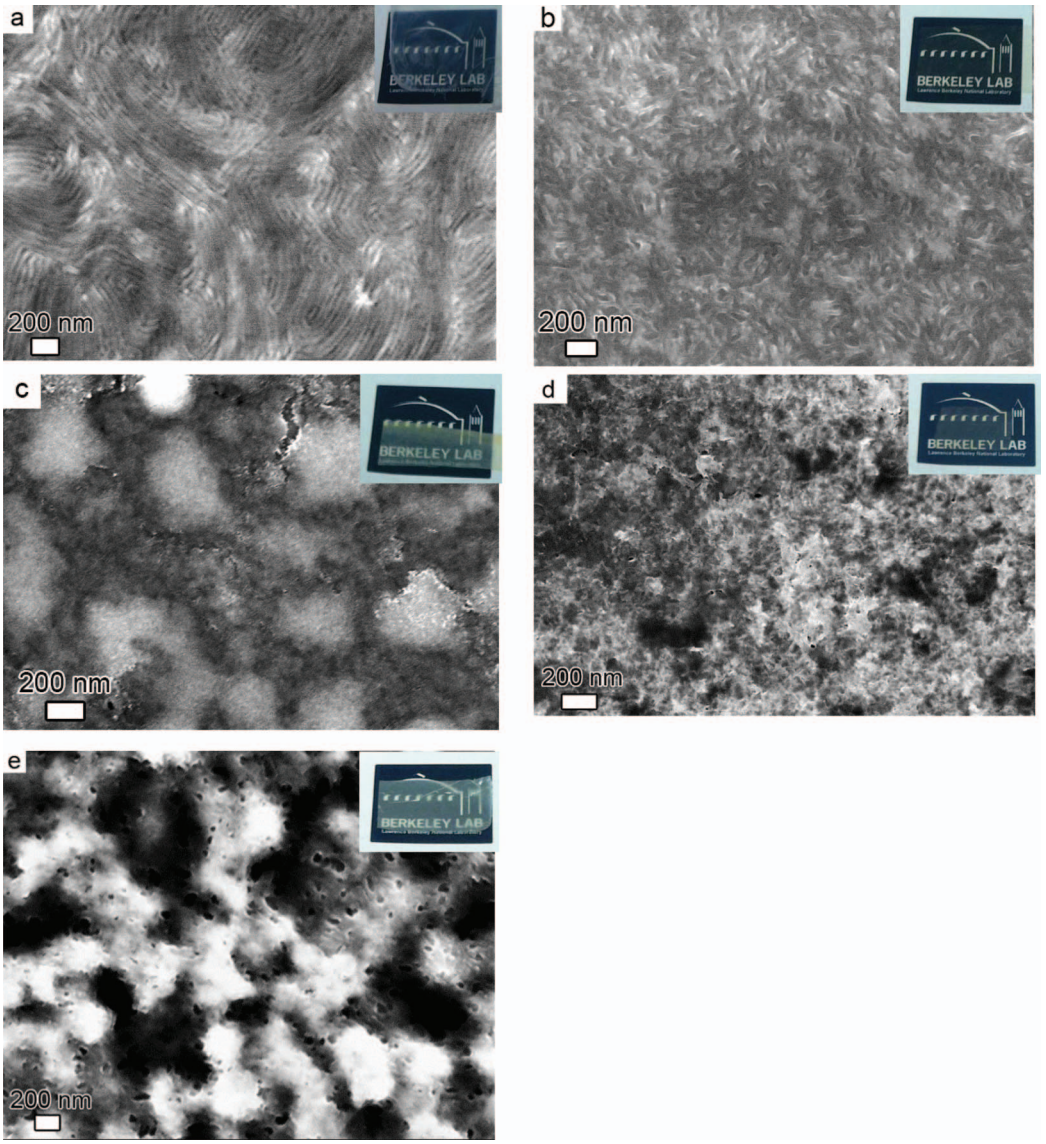


**Figure 2.** SEM micrographs of SEO/LiTFSI/$TiO_2$ electrolytes with different $TiO_2$ contents: 0 wt% (a), 4.3 wt% (b), 11.5 wt% (c), 23.9 wt% (d), 27.9 wt% (e). Bright regions in c-e represent $TiO_2$ clusters. The inserts show images of electrolyte membranes against the same background.

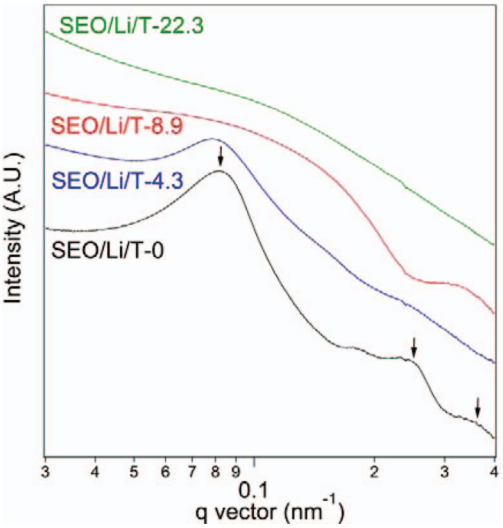


**Figure 3.** RSoXS profiles of SEO/LiTFSI and SEO/LiTFSI/$TiO_2$ mixtures.

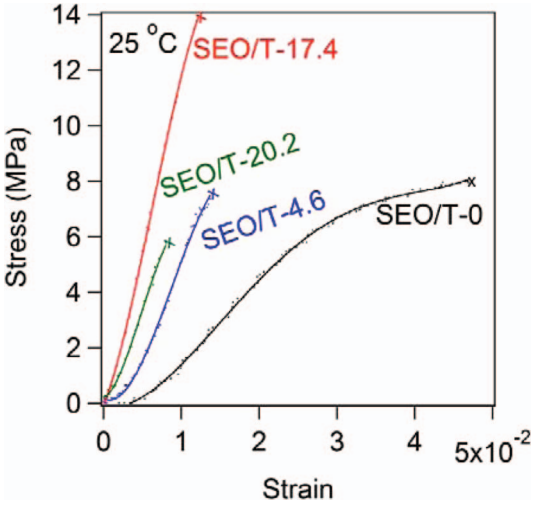


**Figure 4.** Tensile stress-strain curves of SEO and SEO/$TiO_2$ mixtures at room temperature.

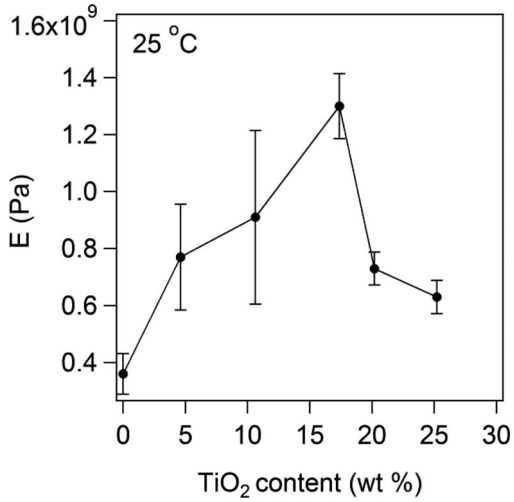


**Figure 5.** Tensile Young moduli of SEO and SEO/$TiO_2$ mixtures versus $TiO_2$ content at room temperature.

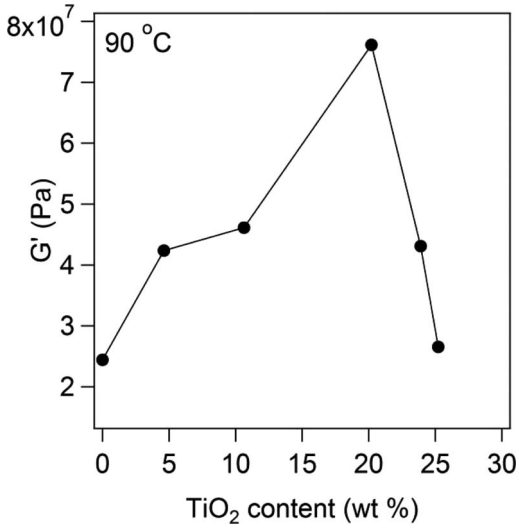


**Figure 7.** Shear storage modulus of SEO and SEO/$TiO_2$ mixtures versus $TiO_2$ content at frequency of 10 Hz, at 90°C.

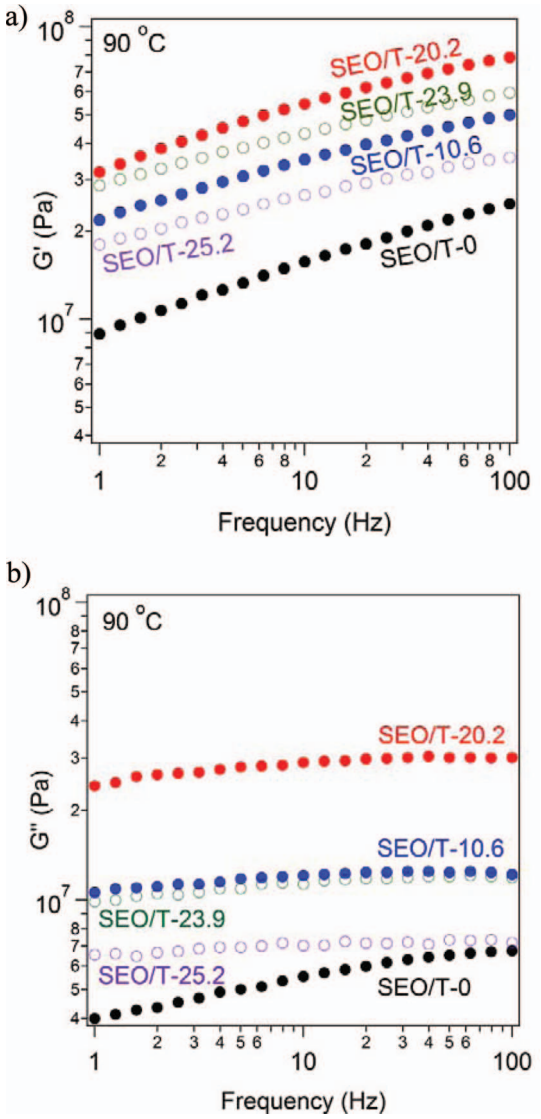


**Figure 6.** Shear moduli as a function of frequency of SEO and SEO/$TiO_2$ mixtures at 90°C: (a) the storage modulus, $G'$ and (b) the loss modulus, $G''$.

Typical results obtained during cycling the symmetric lithium-SEO/Li/T-lithium cells are shown in Figure 9, where data obtained from the last few cycles of a particular cell are shown. The sharp drop in cycling voltage is taken as a signature of a dendrite short,[32–35] and the amount of charge passed until that point per unit area, $C_d$, was recorded for each cell. Figure 10 shows the dependence of $C_d$ on $TiO_2$ content, and the average values are given in Table I. For each set of samples in Figure 10 the error bars represent the variance of the measured $C_d$ values. Adding NPs in the range of 11.5 to 23.9 wt% significantly increased $C_d$ of the composite electrolytes relative to that of the neat SEO/LiTFSI mixture. For instance, $C_d$ increased by a factor of 4.7 in SEO/Li/T-23.9, the optimal composite electrolyte, relative to the unmodified block copolymer. We studied seven SEO/Li/T-23.9 cells. One of them shorted quickly with a $C_d$ value of 336 C/cm$^2$. The six other cells cycled well beyond 1000 C/cm$^2$. This is the only cell wherein the measured $C_d$ value was well outside the standard deviation obtained for the other SEO/LiTFSI/$TiO_2$ cells. We have thus not included the $C_d$ = 336 C/cm$^2$ datum in our analysis. The standard deviation of the measured $C_d$ values for our best membranes is about 500 C/cm$^2$ (Table I). The effect of electrolyte thickness was studied systematically by Hallinan et al. who showed that changing electrolyte thickness from 10 to 30 μm results in an increase in $C_d$

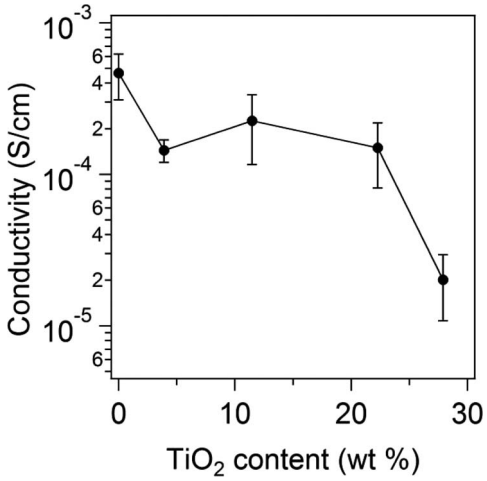


**Figure 8.** Conductivity of SEO/LiTFSI and SEO/LiTFSI/$TiO_2$ electrolytes versus $TiO_2$ content at 90°C.

**Table III. Total charge passed to short circuit for various PEO-based electrolytes normalized by that of pure PEO homopolymer, $C_d/C_{d,PEO}$.**

| Reference | Electrolyte | Current Density (mA/cm$^2$) | Temperature (°C) | $C_d/C_{d,PEO}$ |
|---|---|---|---|---|
| X.-W. Zhang et al.[6] | PEO with Silica | 0.2 and 1.0 | 25 | 1.8 – 5.1 |
| S. Liu et al.[13] | PEO with Silica | 0.1 – 1.0 | 60 | 1.0 – 2.1 |
| S. Liu et al.[14] | PEO with Ionic Liquids | 0.1 – 1.0 | 60 | 1.8 – 3.8 |
| G. M. Stone et al.[21] | Block Copolymer containing PEO | 0.12 – 0.26 | 90 | 11 – 48 |
| SEO/Li/T-0 (this work) | Block Copolymer containing PEO | 0.17 | 90 | 68 |
| SEO/Li/T-23.9 (this work) | Composite Block Copolymer containing PEO and $TiO_2$ | 0.17 | 90 | 321 |

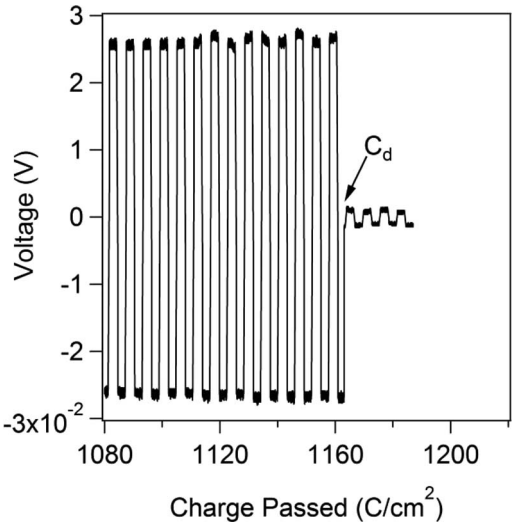


**Figure 9.** Typical voltage versus charge passed curve showing the last cycles for a SEO/Li/T-23.9 electrolyte at 90°C. Total charge passed, $C_d$, before short circuit for this cell due to dendrite formation, is recorded at 1163 C/cm$^2$.

of 200 C/cm$^2$.[36] We thus conclude that differences in the electrolyte thickness are not responsible for the variation of $C_d$ in Figure 10.

Figure 11 shows the relationship between $C_d$ and $G'$. For most cases, higher $C_d$ values were obtained from the electrolyte membranes with higher modulus. The exception is SEO/Li/T-4.3 which has a relatively high value of $G'$, but exhibited relatively poor cycling behavior. This seems to suggest that both morphology and modulus are important parameters in electrolyte design. It is perhaps interesting to note that SEO/Li/T-4.3 was the only ceramic/block copolymer electrolyte that exhibited lamellar morphology (Figure 2b and Figure 3).

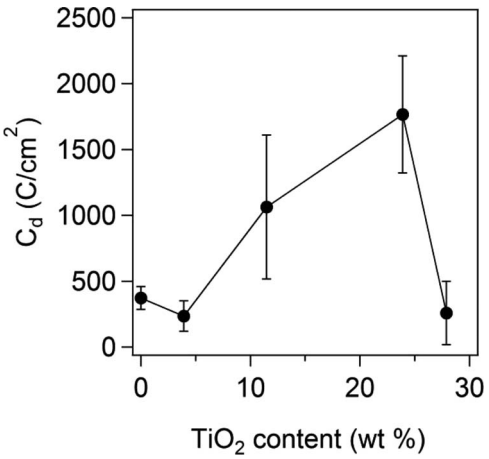


**Figure 10.** Total charge passed to short circuit, $C_d$, for SEO/LiTFSI and SEO/LiTFSI/$TiO_2$ electrolytes versus $TiO_2$ content at 90°C.

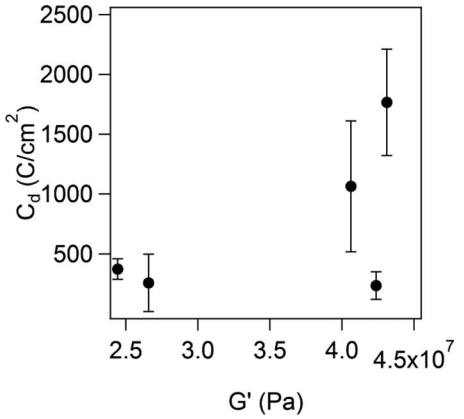


**Figure 11.** Total charge passed to short circuit, $C_d$, as a function of the shear storage modulus, $G'$, for SEO/LiTFSI and SEO/LiTFSI/$TiO_2$ electrolytes at 90°C.

In Table III we compare the $C_d$ values of selected composite electrolytes studied in this paper with previously published data.[6,13,14,21] This comparison is facilitated by examining the value of $C_d$ obtained in electrolyte of interest in electrolyte of interest, normalized by that of pure PEO-based electrolyte, $C_d/C_{d,PEO}$. The $C_{d,PEO}$ value used in the last two entries in Table III are taken from Ref. 21. The addition of silica and ionic liquids to PEO electrolytes results in $C_d/C_{d,PEO}$ ranging from 1.0 to 5.1 (Table III). The $C_d/C_{d,PEO}$ of SEO/Li/T-0, which is 68, is slightly higher than the $C_d/C_{d,PEO}$ reported by Stone et al. for SEO-based electrolytes.[21] We speculate that this is due to improvements in cell building procedures. The $C_d/C_{d,PEO}$ of the optimal composite electrolyte, SEO/Li/T-23.9, is 321.

## Conclusions

We have shown that the addition of $TiO_2$ nanoparticles to SEO/LiTFSI block copolymer electrolytes can significantly inhibit dendrite growth on lithium metal electrodes. The most stable performance in symmetric lithium-composite electrolyte-lithium cells was found in composite electrolytes with about 24 wt% NPs. The amount of charge passed before short circuit due to dendrite formation increased by a factor of 4.7, relative to that of the neat block copolymer electrolyte. In contrast, the conductivity of all of the composite electrolytes was lower than that of the SEO/LiTFSI mixture without NPs. Thus, conductivity differences do not explain the observed stability of NP-containing electrolytes. The reason for the improved performance is the morphology and mechanical properties of the composite. At about 20 wt% NPs we find that the composite electrolytes are transparent (Table I), SEM micrographs show neither clustering of $TiO_2$ NPs nor the existence of the lamellar morphology (Figure 2), and both tensile and shear moduli are maximized (Figures 5 and 7). There appears to be a correlation between the stability of the NP-containing block copolymer electrolytes, morphology, and mechanical properties.

## Acknowledgments

The synthesis, preparation, conductivity measurements and cycling experiments of the composite polymers were supported by the Assistant Secretary for Energy Efficiency and Renewable Energy, Office of Vehicle Technologies of the U.S. Department of Energy under Contract DE-AC02-05CH11231 under the Batteries for Advanced Transportation Technologies (BATT) Program. RSoXS experiments were performed at the Advanced Light Source, transmission electron microscopy was performed at the National Center for Electron Microscopy, $TiO_2$ synthesis, scanning electron microscopy and TGA experiments were performed at the Molecular Foundry, mechanical testing were performed at the Division of Materials Sciences, all user facilities at Lawrence Berkeley National Laboratory supported by the Director, Office of Science, Office of Basic Energy Sciences, Division of Materials Sciences and Engineering, of the U.S. Department of Energy under Contract No. DE-AC02-05CH11231. We thank Dr. Michel Foure for suggesting the project.

## List of Symbols

| | |
|---|---|
| $C_d$ | total charge passed before short circuit (C/cm$^2$) |
| $C_d/C_{d,PEO}$ | $C_d$ obtained in electrolyte of interest normalized by that of pure PEO-based electrolyte |
| $G'$ | shear storage modulus (Pa) |
| $G''$ | shear loss modulus (Pa) |
| $E$ | tensile Young modulus (Pa) |
| $q$ | scattering vector (nm$^{-1}$) |

## Greek

| | |
|---|---|
| $\lambda$ | wavelength of X-rays |
| $\theta$ | scattering angle of X-rays |

## References

1. J. M. Tarascon and M. Armand, *Nature*, **414**(6861), 359 (2001).
2. D. Devaux, R. Bouchet, D. Glé, and R. Denoyel, *Solid State Ionics*, **227**(0), 119 (2012).
3. M. Armand, *Solid State Ionics*, **9-10**, **Part 2** (0), 745 (1983).
4. D. Baril, C. Michot, and M. Armand, *Solid State Ionics*, **94**(1–4), 35 (1997).
5. G. S. MacGlashan, Y. G. Andreev, and P. G. Bruce, *Nature*, **398**(6730), 792 (1999).
6. X.-W. Zhang, Y. Li, S. A. Khan, and P. S. Fedkiw, *Journal of The Electrochemical Society*, **151**(8), A1257 (2004).
7. C. Monroe and J. Newman, *Journal of The Electrochemical Society*, **152**(2), A396 (2005).
8. F. Croce, G. B. Appetecchi, L. Persi, and B. Scrosati, *Nature*, **394**(6692), 456 (1998).
9. W. Wieczorek, K. Such, S. H. Chung, and J. R. Stevens, *The Journal of Physical Chemistry*, **98**(36), 9047 (1994).
10. W. Krawiec, L. G. Scanlon Jr, J. P. Fellner, R. A. Vaia, S. Vasudevan, and E. P. Giannelis, *Journal of Power Sources*, **54**(2), 310 (1995).
11. B. Scrosati, *The Chemical Record*, **1**(2), 173 (2001).
12. D. Golodnitsky, G. Ardel, and E. Peled, *Solid State Ionics*, **147**(1-2), 141 (2002).
13. S. Liu, N. Imanishi, T. Zhang, A. Hirano, Y. Takeda, O. Yamamoto, and J. Yang, *Journal of Power Sources*, **195**(19), 6847 (2010).
14. S. Liu, N. Imanishi, T. Zhang, A. Hirano, Y. Takeda, O. Yamamoto, and J. Yang, *Journal of The Electrochemical Society*, **157**(10), A1092 (2010).
15. K. Takahashi, J. Ohmura, D. Im, D. J. Lee, T. Zhang, N. Imanishi, A. Hirano, M. B. Phillipps, Y. Takeda, and O. Yamamoto, *Journal of The Electrochemical Society*, **159**(4), A342 (2012).
16. J. L. Schaefer, S. S. Moganty, D. A. Yanga, and L. A. Archer, *Journal of Materials Chemistry*, **21**(27), 10094 (2011).
17. Y. Lu, S. K. Das, S. S. Moganty, and L. A. Archer, *Advanced Materials*, **24**(32), 4430 (2012).
18. A. Panday, S. Mullin, E. D. Gomez, N. Wanakule, V. L. Chen, A. Hexemer, J. Pople, and N. P. Balsara, *Macromolecules*, **42**(13), 4632 (2009).
19. M. Singh, O. Odusanya, G. M. Wilmes, H. B. Eitouni, E. D. Gomez, A. J. Patel, V. L. Chen, M. J. Park, P. Fragouli, H. Iatrou, N. Hadjichristidis, D. Cookson, and N. P. Balsara, *Macromolecules*, **40**(13), 4578 (2007).
20. W.-S. Young and T. H. Epps, *Macromolecules*, **45**(11), 4689 (2012).
21. G. M. Stone, S. A. Mullin, A. A. Teran, D. T. Hallinan, A. M. Minor, A. Hexemer, and N. P. Balsara, *Journal of The Electrochemical Society*, **159**(3), A222 (2012).
22. S. Kalnaus, A. S. Sabau, W. E. Tenhaeff, N. J. Dudney, and C. Daniel, *Journal of Power Sources*, **201**(0), 280 (2012).
23. A. Dong, X. Ye, J. Chen, Y. Kang, T. Gordon, J. M. Kikkawa, and C. B. Murray, *Journal of the American Chemical Society*, **133**(4), 998 (2011).
24. R. Buonsanti, E. Carlino, C. Giannini, D. Altamura, L. De Marco, R. Giannuzzi, M. Manca, G. Gigli, and P. D. Cozzoli, *Journal of the American Chemical Society*, **133**(47), 19216 (2011).
25. D. T. Wong, C. Wang, K. M. Beers, J. B. Kortright, and N. P. Balsara, *Macromolecules*, **45**(22), 9188 (2012).
26. J. M. Virgili, Y. Tao, J. B. Kortright, N. P. Balsara, and R. A. Segalman, *Macromolecules*, **40**(6), 2092 (2007).
27. Z. Huo, C.-K. Tsung, W. Huang, M. Fardy, R. Yan, X. Zhang, Y. Li, and P. Yang, *Nano Letters*, **9**(3), 1260 (2009).
28. E. Ploshnik, A. Salant, U. Banin, and R. Shenhar, *Physical Chemistry Chemical Physics*, **12**(38), 11885 (2010).
29. E. Ploshnik, A. Salant, U. Banin, and R. Shenhar, *Advanced Materials*, **22**(25), 2774 (2010).
30. J. Gutierrez, A. Tercjak, and I. Mondragon, *Journal of the American Chemical Society*, **132**(2), 873 (2010).
31. W.-C. Yen, Y.-H. Lee, J.-F. Lin, C.-A. Dai, U. S. Jeng, and W.-F. Su, *Langmuir*, **27**(1), 109 (2011).
32. J.-N. Chazalviel, *Physical Review A*, **42**(12), 7355 (1990).
33. M. Rosso, C. Brissot, A. Teyssot, M. Dollé, L. Sannier, J.-M. Tarascon, R. Bouchet, and S. Lascaud, *Electrochimica Acta*, **51**(25), 5334 (2006).
34. C. Brissot, M. Rosso, J. N. Chazalviel, P. Baudry, and S. Lascaud, *Electrochimica Acta*, **43**(10-11), 1569 (1998).
35. C. Brissot, M. Rosso, J. N. Chazalviel, and S. Lascaud, *Journal of Power Sources*, **81-82**(0), 925 (1999).
36. D. T. Hallinan, S. A. Mullin, G. M. Stone, and N. P. Balsara, *Journal of The Electrochemical Society*, **160**(3), A464 (2013).